Light-Driven Wettability Changes on a Photoresponsive Electrospun Mat

Menglin Chen[†,*] and Flemming Besenbacher[†,‡]

[†]Interdisciplinary Nanoscience Center (iNANO) and [‡]Department of Physics and Astronomy (IFA), Aarhus University, DK-8000 Aarhus C, Denmark

ABSTRACT Novel nanofibers of biodegradable polycaprolactone (PCL) modified with light-responsive azobenzene were prepared by electrospinning upon a facile one-pot reaction. The surface chemistry of the nanofibers was probed by X-ray photoelectron spectroscopy (XPS) and time-of-flight secondary ion mass spectrometry (ToF-SIMS). Both XPS and ToF-SIMS spectra proved the successful conjugation of azobenzene with PCL. ToF-SIMS not only enabled chemical mapping but also provided morphology information, supplementary to scanning electron microscopy (SEM). The large, reversible, and light-responsive wettability changes of the functional fibrous surfaces were further demonstrated using UV−vis spectroscopy and contact angle (CA) measurements.

KEYWORDS: nanofibers · light-responsive · electrospinning · wettability

Functional surfaces with controllable wettabilities upon external stimulus[1−8] have come to the forefront of research, providing many new possibilities for biological and industrial applications.[9,10] A particularly intriguing possibility is offered by light-responsive materials allowing remote and accurate operation that can easily be focused into specific areas of applications. The photoresponse of these materials is based on the photoisomerization of constituent molecules that undergoes a large conformational change between two states in response to the absorption of light at two different wavelengths.[11] Typically, *trans*−*cis* isomerization of azobenzene chromophores,[12] which reversibly interconverts between an extended, thermally relaxed *trans* isomer and a higher energy *cis* or "bent" isomer that is ∼0.7 nm shorter than the *trans* isomer without detectable photodestruction or loss of responsiveness,[13] gives rise to changes of the dipole moments, polarity, or shape of the molecules. Thus, these azobenzene chromophores open up limitless utilizations in the synthesis of intelligent materials, such as liquid crystals with great promise in actuators, sensors, micromachines, and artificial muscles,[14−17] 3D ordered polymer brushes for photomechanical soft materials,[18] nanoparticles for data storage and photoregulated synthesis,[13,19−21] dendrimers for light harvesting and responsive polymersomes,[22,23] supramolecular helix for photodynamic systems,[24] and photochromic ligands for cell signaling.[13]

Apart from modifying the surface chemistry, the surface wettability can also be tuned by altering the surface topography. Different azobenzene-contained thin films were fabricated using chemsorption,[25] the Langmuir−Blodgett (LB) technique[26] or self-assembly, on which only limited changes of water contact angle (CA) about 10° were observed until electrostatic layer-by-layer deposition was utilized in combination with photolithography[27] or hydrophobic surfaces.[28] Compared with the change of CA on the flat thin films (only about 2°), a large change of the water CA of about 66° was induced on a rough, 40 μm pillar spacing silicon substrate.[27]

Electrospinning is a remarkably robust and versatile method for fabricating fibers with diameters down to the nanometer length scale.[29] Electrospinning has become particularly powerful in widely different areas[30,31] when its surface features of the nanofibers are combined with easy add-on functions. Not surprisingly, the induced topographic nanostructure roughness might intrinsically contribute to the stimuli-responsive wettabilities, such as thermo-responsive PNIPAAm-contained fibrous surfaces.[7]

Herein we report the first study of light-responsive electrospun azobenzene-modified polycaprolactone (PCL-azo) nanofibers (Figure 1). Polycaprolactone (PCL) as a biodegradable and biocompatible linear polyester with potential use in tissue engineering[32] and drug delivery[33] was chosen as the polymer carrier. Instead of labor-intensive synthesis of azobenzene PCL copolymers, a one-pot synthesis was applied using benzophenone-4-isothiocyanate (BPITC) as a well-known heterobifunctional, photoreactive cross-linker.[34]

The surface chemistry of the nanofibers was quantified with X-ray photoelectron spectroscopy (XPS). Time-of-flight secondary ion mass spectrometry (ToF-SIMS)

*Address correspondence to menglin@inano.au.dk.

Received for review December 23, 2010 and accepted January 10, 2011.

Published online February 02, 2011
10.1021/nn103577g

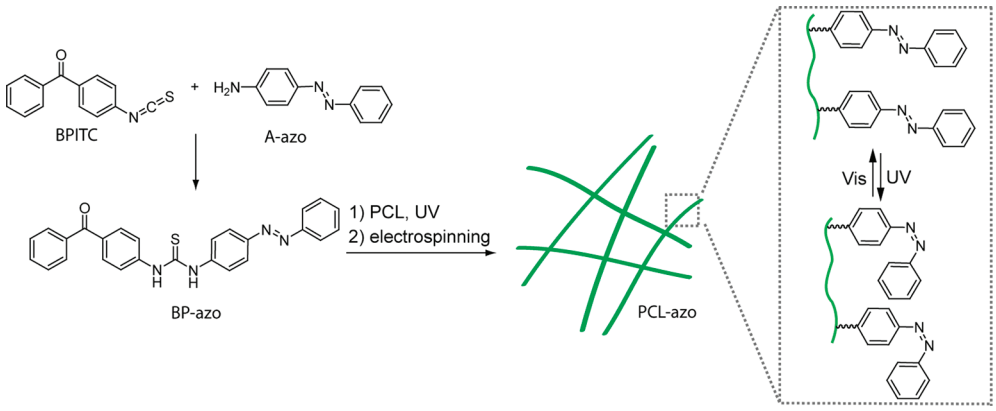

Figure 1. Schematic illustration of electrospinning of PCL-azo and the produced light-responsive nanofibers.

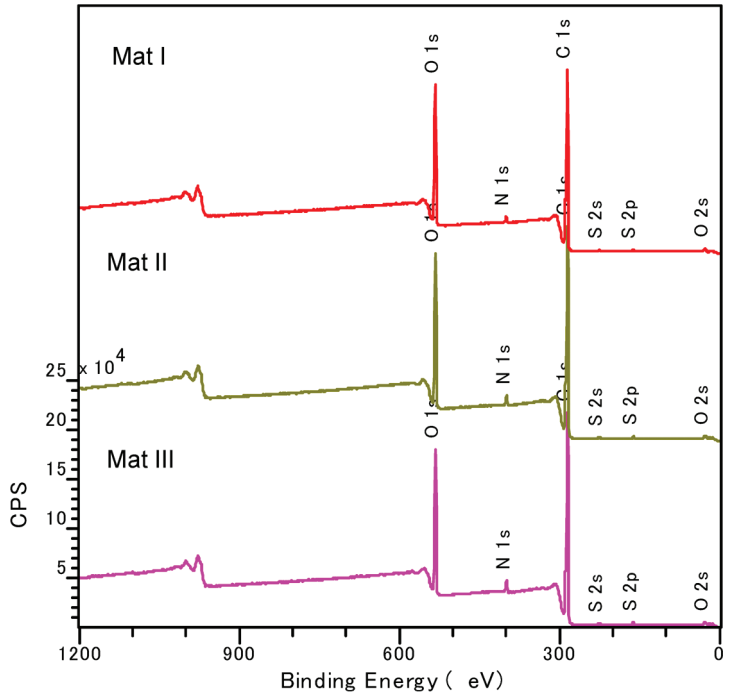

Figure 2. XPS wide scan spectra of mat I, BP-azo/PCL = 3.5%/20%; mat II, Bp-azo/PCL = 5%/20%; mat III, BP-azo/PCL = 6.7%/20%.

was utilized both for chemical mapping and for offering topological information, supplementary to scanning electron microscopy (SEM). The photoresponsibility of the fibers was subsequently investigated using UV−vis spectroscopy and contact angle (CA) measurements.

RESULTS AND DISCUSSION

Fabrication of PCL-Azo Electrospun Nanofibers. The conjugation of azobenzene with PCL was performed in a one-pot reaction (Figure 1). Amino-functionalized azobenzene A-azo and PCL were chosen as the starting materials. The heterobifunctional, photoactive cross-linker, BPITC, with an isothiocyanate group reactive to aromatic amines and benzophenone species ready for C−H insertion in PCL upon UV illumination, was reacted with excess of A-azo first to form BP-azo and subsequently with PCL. Thus, the modified polymer PCL-azo having PCL as the linear main chains and BP-azo as the branch side chains was formed. Three nanofibrous mats with different azobenzene concentrations were obtained upon electrospinning: mat I, BP-azo/PCL = 3.5 w/v %/20 w/v %; mat II, BP-azo/PCL = 5 w/v %/20 w/v %; and mat III, BP-azo/PCL = 6.7 w/v %/20 w/v %. The unreacted A-azo molecules were easily removed in the vacuum.

XPS Quantification. The wide energy survey XPS scans depicted in Figure 2 demonstrate that the fibrous surfaces of the nanofibers consist of carbon, oxygen, sulfur, and nitrogen, where sulfur and nitrogen come from BP-azo fragments only.

Since XPS provides quantitative information of components present in the outer molecular layers, the surface concentration of azobenzene tethered to PCL (labeled % azo) can be determined. Theoretically, the ratio between [N], [O], [S], and [C] in BP-azo side chains ($C_{26}H_{21}N_4OS$) is [N]/[O]/[S]/[C] = 4/1/1/26. Therefore, from the wide energy survey scans, % azo = (26 + 1 + 1 + 4)/4 × N% = 8 × N% (Table 1, method a), or % azo =32 × S% (Table 1, method b). It shows that the contents of azobenzene molecules on the surfaces are consistent with those in the stock solutions, which demonstrates that BP-azo has been successfully conjugated with PCL with nearly 90% yield in the one-pot reaction and has been well-dispersed in the nanofibers upon electrospinning.

ToF-SIMS Chemical Mapping and SEM Imaging. While XPS determined the elemental composition of the PCL-azo fibrous surfaces, ToF-SIMS was applied to identify the chemical species and to map their distribution on the surfaces of individual nanofibers with a depth resolution of 1−2 nm. The positive ion spectrum for the mat III (BP-azo/PCL = 6.7%/20%) with the highest BP-azo dosage (Figure 4) clearly shows both signals from PCL main chains, such as *m/z* 55 ($C_3H_3O^+$), *m/z* 69 ($C_5H_9^+$), and *m/z* 115 ($C_6H_{11}O_2^+$, monomer), and signals from BP-azo side chains, such as *m/z* 77 ($C_6H_5^+$), *m/z* 105 ($C_6H_5N_2^+$), *m/z* 405 ($C_{26}H_{21}N_4O^+$), *m/z* 437 ($C_{26}H_{21}N_4OS^+$, monomer), and *m/z* 448 ($C_{27}H_{20}N_4OS^+$).

The identified fragment ions originating from either BP-azo side chains or PCL main chains (Figure 3) appear at unique nominal *m/z* values. They can thus be used to obtain chemical maps of the distribution of BP-azo side chains and PCL main chains on the fiber surfaces. Individual nanofibers in the mat I (BP-azo/PCL = 3.5%/20%), mat II (BP-azo/PCL = 5%/20%), and mat III (BP-azo/PCL = 6.7%/20%) were imaged using the chemical contrasts observed (Figure 4a−c), and their surface roughness was estimated using 3D images (Figure 4d). The observations are consistent with all mats I−III, confirming that the surface concentrations of BP-azo tethered to PCL increased as the dosages increased, supporting the XPS data.

As shown in the SEM images of the electrospun fiber mats I−III (Figure 4e), the diameters of the nanofibers increased from 365 ± 132 nm (mat I) to 871 ± 125 nm (mat III) along with the increase of BP-azo dosage. This is in accordance with an increase of the viscosity due to the higher conjugation of BP-azo giving rise to a higher number of chain entanglements. The viscosity also affects the evaporation rate of the solvent: at high viscosities, solvent evaporation of solvent is slow, allowing the collected wet fibers to weld together and form a cross-linking structure during solidification, as shown in mat III.

Photoresponsibilities. Azobenzene-functionalized PCL (PCL-azo) exhibited an intense absorbance at about 352 nm before UV irradiation corresponding to the $\pi-\pi^*$ transition band of the *trans* isomer (Figure 5). Upon UV light irradiation (365 nm, I_{UV} = 15 mW cm^{-2}, 1 h), a weak band at about 453 nm related to n−π^* transition band of the *cis*-azobenzene appeared, while the intensity of $\pi-\pi^*$ transition band at 352 nm decreased, indicating a transition from the *trans* state to the *cis* isomerized state, whereby approximately 30% of the population is transferred from the *trans* state to the *cis*; upon the visible light irradiation, the *trans* was recovered. Absorbance at 302 nm related to the benzophenone species has red-shifted to 314 nm

TABLE 1. Atomic Concentration Generated by Wide Scan and Surface Composition of Azobenzene

	atomic concentration generated by wide scan (%)				% azo	
mat	C	N	O	S	solution	surface
I	62.51	1.66	35.41	0.42	15%	13.3%[a], 13.4%[b]
II	61.12	2.24	36.09	0.55	20%	17.9%[a], 17.6%[b]
III	59.70	2.78	36.82	0.70	25%	22.2%[a], 22.4%[b]

[a] Method a: % azo = 8 × N%. [b] Method b: % azo = 32 × S%

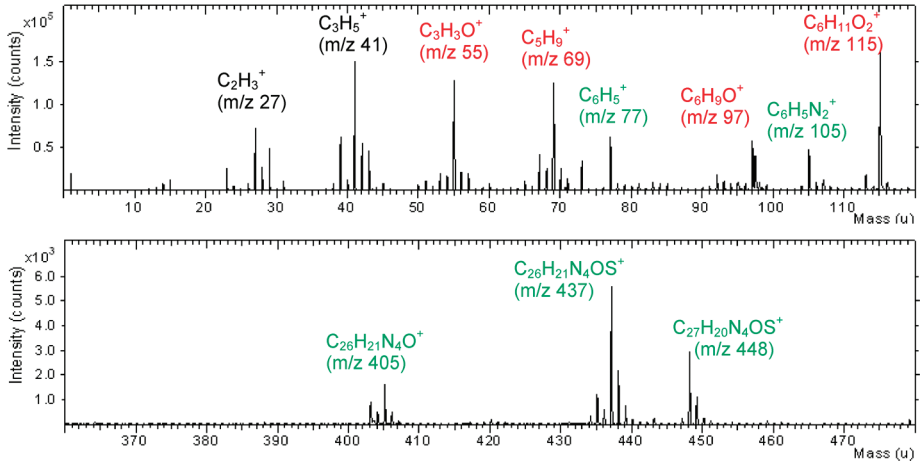

Figure 3. Representative positive ion ToF-SIMS spectra recorded from the mat III, BP-azo/PCL = 6.7%/20%. Major peaks assignments for PCL are shown in red and for BP-azo fragments in green.

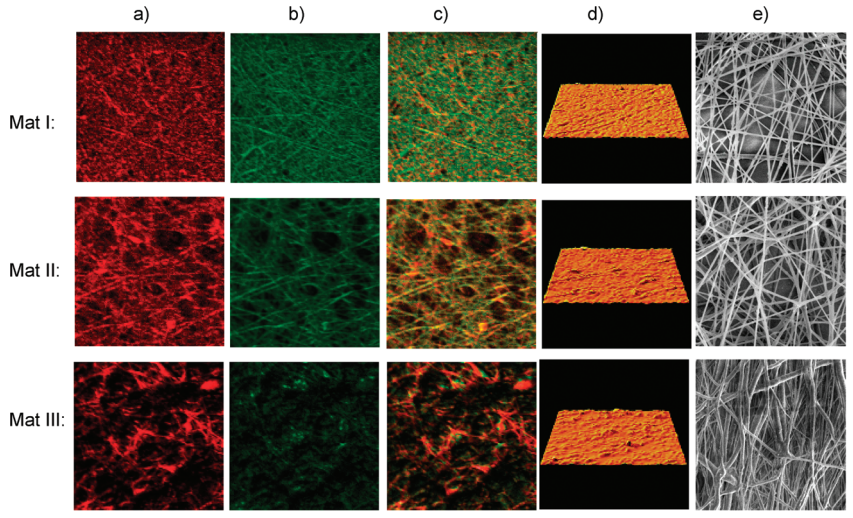

Figure 4. ToF-SIMS chemical images and SEM images of the nanofibrous mats I–III. (a) Azobenzene fragment ion images; (b) PCL fragment ion images; (c) overlay images of column (a) and column (b); (d) 3D images of total ions; (e) SEM images. Area: 20 μm × 20 μm.

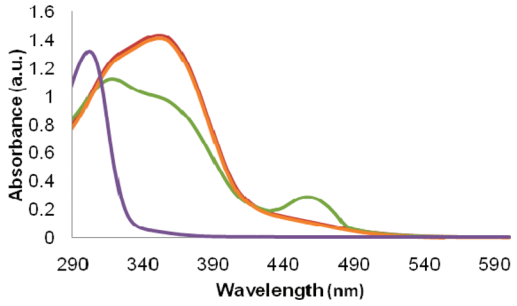

Figure 5. UV–vis absorption spectra of polymer PCL-azo synthesized from solution III (BP-azo/PCL = 6.7%/20%). Red: before UV irradiation. Green: after UV irradiation 1 h. Orange: after visible light irradiation 15 min. Blue: compound BPITC.

upon conjugation with PCL, which again proved the successful formation of PCL-azo.

Since the surface free energies of flat solid substrates are determined by atomic level constitutions of their outermost surfaces,[35,36] an alteration of the chemical structures of the outermost monomolecular layers by light can be used to trigger and manipulate various interfacial phenomena, including the surface wettability of the nanofibers.[37,38]

To discern whether the photoresponsibility of azobenzene is retained in the electrospun fibers, water contact angle (CA) static/dynamic measurements upon UV/vis irradiation were performed, and static CA together with advancing angle (θ_A)/receding angels (θ_R) were recorded. All mats turned from yellow to orange upon UV irradiation (365 nm, I_{UV} = 15 mW cm^{-2}, 1 h), according to the absorbance of the *cis*-azobenzene; no bending or significant surface morphology changes were observed. Mat I (BP-azo/PCL = 3.5%/20%) demonstrated a static CA alteration from 121.3 ± 3.2° (θ_A = 124.5 ± 2.0°, θ_R = 110.1 ± 5.2°) to 90.6 ± 2.8° (θ_A = 95.3 ± 3.0°, θ_R = 80.2 ± 5.0°) upon UV irradiation. A larger static CA alteration was obtained from mat II (BP-azo/PCL = 5.0%/20%), where CA changed from 127.3 ± 2.7° (θ_A = 130.5 ± 2.1°, θ_R = 116.1 ± 4.2°) to 78.2 ± 3.8° (θ_A = 82.1 ± 2.8°, θ_R = 60.5 ± 4.8°) upon UV irradiation. Mat III (BP-azo/PCL = 6.7%/20%) showed the most significant static CA change; the CA of mat III decreased from 132.2 ± 2.8° (θ_A = 137.1 ± 2.5°, θ_R = 113.1 ± 4.5°) to 53.1 ± 3.2° (θ_A = 57.2 ± 2.3°, θ_R = 32.6 ± 4.7°) upon UV irradiation. The wettability changes switched back after exposure under visible light (15 min). These photoswitch phenomena were found to be reversible for a few cycles (Figure 6).

The changes observed upon UV irradiation were due to the reversible *trans*-to-*cis* isomerization of the azobenzene groups. This *trans*-to-*cis* isomerization caused an increase of the dipole moment of the azobenzene molecules ($\mu \approx 5$ debye for the *cis* form *vs* $\mu \approx 1$ debye for the *trans* isomer[39]), which causes a lowering of the surface free energy and thus a more hydrophilic surface. An increased dosage of azobenzene on the surface induced a larger lowering of the surface free energy upon *trans*-to-*cis* isomerization and consequently a lower water CA.

Apart from the chemical nature of surfaces, roughness also plays an important role for wetting behavior, where the Wenzel and Cassie theories are commonly applied.[40,41] Microstructures,[27] nanostructures,[42,43] and nano/micrometer dual-topography structures[44–46] have been synthesized to modulate stimuli-responsive wettabilities.

A size-dependent effect has been revealed for a micropillar patterned template with different (5–60 μm) spacing[27] and a nanopore patterend template with different (0–200 nm) pore size,[43] where 40 μm spacing pillars and 200 nm pores, respectively, were found to enhance the wettabilities most significantly. Instead of homogeneous microscale or nanoscale

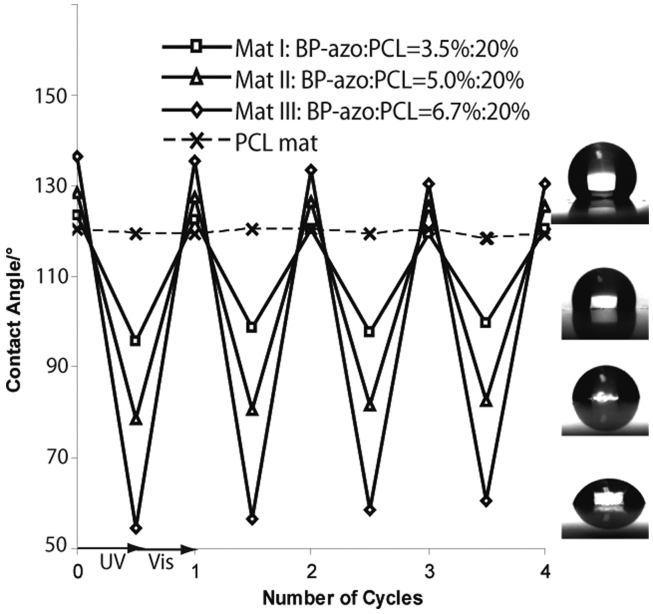

Figure 6. Photographs of water droplet shape and on the mats I−III, which show that photoresponsive wettabilities could reversibly switch between hydrophobicity and hydrophilicity upon UV/vis irradiation. PCL mat without azobenzene displayed no photoresponse but hydrophobic nature.

systems, a detailed study of nano/micrometer dual-topography structures[44] with varied sizes of both nanopillars and micropillars was attempted and successfully proved that the hierarchical structures are crucial to obtain a stable Cassie state with a high CA as well as a low CA hysteresis.

Electrospun mats deposited on stationary collectors are generally randomly aligned and contain nano/microscale fibers, beads, and pores. They are thus rather complex hierarchical systems compared to the above-mentioned nanoengineered ordered models. Similar to the electrospun PS/PNIPAAm fibers,[45] with their microbead/nanofiber hierarchical structure being claimed to contribute to the thermoresponsive wettabilities, we believe the nanofiber/micropore dual topography in our electrospun azobenzene-contained mats also amplifies the wettability changes.

Furthermore, the thorough study of the nanopores[43] indicated that the size of nanopores might vary upon stimuli, which could be another origin of the wettability changes. Although no significant micropore size changes were obtained upon UV irradiation, considering the fact and the nanomechanic application[14−17] of that the *cis* or "bent" isomer is ~0.7 nm shorter than the *trans* isomer,[13] and the observed, slightly changed CA hysteresis ($\theta_A - \theta_R$), nanoscale morphology changes on the individual fiber surfaces might occur, which could further alter the wettabilities. Further experiments of *in situ* nanoscale morphology studies are under development.

The large, reversible, and light-responsive wettability changes associated with azobenzene photoisomerization allow us to control the properties and the function of the nanofibers with light, which opens up for a lot of interesting and visionary applications.

CONCLUSIONS

We have presented the first study of electrospun PCL-azo nanofibers. Biodegradable polycaprolactone (PCL) was modified with light-responsive azobenzene through a facile one-pot reaction. Different nanofibrous mats with different concentrations of BP-azo tethered to PCL were produced by electrospinning. While XPS quantified the surface concentrations of azobenzene molecules tethered to PCL, ToF-SIMS, a powerful surface analysis technique, enabled intuitive chemical distribution imaging together with the available topological information.

The well-known *trans−cis* isomerization of azobenzene under the trigger of light at different wavelengths caused a significant change of the dipole moment and subsequently the surface free energy. The exhibited large, reversible, and light-responsive wettability changes, which were demonstrated using UV−vis spectroscopy and contact angle (CA) measurements, arise not only from the azobenzene surface functionalization but also from the roughness intrinsically offered by the electrospun nano/microscale hierarchical structures.

We believe the combination of the photoresponsibility from azobenzenes and the biodegradability from PCL in a nanofibrous manner may flourish their potential in drug delivery, tissue engineering, sensors,

and optical storage. Furthermore, this present novel study again proved electrospinning's simplicity, robustness, and versatility with intrinsic nanofeatures, extending its great potential in a broad range of research fields.

EXPERIMENTAL SECTION

Materials. Benzophenone-4-isothiocyante (BPITC) was purchased from Invitrogen. Polycaprolactone (PCL) (M_w = 80 000), 4-aminoazobenzene (A-azo), chloroform, and dimethylformamide (DMF) were purchased from Sigma-Aldrich. The materials were used without any purification.

One-Pot Synthesis of PCL-Azo and Electrospinning. A solution of A-azo (236 mg, 1.2 mmol) and BPITC (239 mg, 1 mmol) dissolved in 1 mL of DMF was stirred overnight at room temperature. The completion of the reaction was confirmed by thin layer chromatography (TLC). A solution of 25 w/v % PCL in 0.8 mL of chloroform was then added to three different amounts of the reaction solution: 80 μL (I), 115 μL (II), and 154 μL (III). After filling up the three solutions with DMF to a total volume of 1 mL, the final w/v concentrations of solutions are (I) BP-azo/PCL = 3.5 w/v %/20 w/v %, (II) BP-azo/PCL = 5 w/v %/20 w/v %, and (III) BP-azo/PCL = 6.7 w/v %/20 w/v %, in DMF/chloroform (1:4), assuming the yield of BP-azo was 100%.

The homogeneous polymer solutions were exposed under UV light using Spectroline Optimax 365 LED UV lamp (365 nm, I_{UV} = 15 mW cm^{-2}) for 2 h before placed in a 1 mL syringe fitted with a metallic needle of 0.4 mm inner diameter. The syringe was fixed horizontally on the syringe pump (model KDS 101, KD Scientific), and an electrode of high voltage power supply (Spellman High Voltage Electronics Corporation, MP Series) was clamped to the metal needle tip. The flow rate of polymer solution was 1 mL/h, and the applied voltage was 18 kV. The tip-to-collector distance was set to 12 cm between a grounded stationary and a rectangular metal collector (15 cm × 20 cm). The collected fibrous mats I−III were collected on Al foils for 20 min and then dried in vacuum at 40 °C overnight to remove any remaining starting compounds and solvents.

Measurements and Characterization. X-ray photoelectron spectroscopy (XPS) was performed using a Kratos Axis Ultra^{DLD} instrument equipped with a monochromated Al Kα X-ray source ($h\nu$ = 1486.6 eV) operating at 15 kV and 15 mA (225 W). A hybrid lens mode was employed during analysis (electrostatic and magnetic), with an analysis area of approximately 300 μm × 700 μm. For each sample, a takeoff angle (TOA) of 0° (with respect to the sample surface) was used, allowing maximum probe depth (10 nm). Wide energy survey scans (WESS) were obtained over the range of 0−1200 eV binding energy (BE) at a pass energy of 160 eV and used to determine the surface elemental composition.

Time-of-flight secondary ion mass spectroscopy (ToF-SIMS) analysis was performed using an ION-TOF TOF SIMS 5 instrument equipped with a Bi primary ion cluster source operating at 25 kV. In most cases, Bi^{3+} primary ions were used with a target current of 0.3 pA. High-resolution mass spectra ($M/\Delta M$ > 4000 at m/z = 27) were acquired using the high current bunched mode. High mass resolution spectra were obtained by the use of bunched primary ions. The analysis area was 500 μm × 500 μm. Only positive secondary ion spectra were acquired, and mass calibration of the spectra was based on CH_3^+, $C_2H_3^+$, and $C_3H_5^+$ ions. Chemical imaging was performed with the burst alignment mode, which offers a high spatial resolution but low mass resolution. Due to the low mass resolution, chemical imaging was based only on peaks unambiguously identified from high mass resolution spectra over an area of 20 μm × 20 μm. In all cases, an electron flood gun was for charge compensation and the primary ions dose was kept below 10^{12} ions/cm^2 to stay within the *static* SIMS regime.

The surface morphology of the electrospun nanofibers was examined by high-resolution scanning electron microscopy (SEM) (FEI, Nova 600 NanoSEM) at 5 kV.

The UV−vis spectra of diluted solutions I−III and compound BPITC were recorded on a Shimadzu UV-3600 UV−vis−NIR spectrophotometer.

The contact angle (CA) was measured by means of a Krüss Drop Shape Analysis System DSA100. The light-controlled experiments were performed using Spectroline Optimax 365 LED UV lamp (365 nm, I_{UV} = 15 mW cm^{-2}). The average CA values were obtained by measuring five different positions on the same sample.

Acknowledgment. We gratefully acknowledge the funding to the current project NanoNonwovens from The Danish National Advanced Technology Foundation, the collaboration with Fibertex A/S, the Danish Research Agency for the funding to the iNANO Center and the Lundbeck and the Carlsberg Foundations for their financial support. Charlotte Illum Nielsen is sincerely acknowledged for proofreading of the manuscript.

REFERENCES AND NOTES

1. Russell, T. P. Surface-Responsive Materials. *Science* **2002,** *297*, 964–967.
2. Yu, X.; Wang, Z. Q.; Jiang, Y. G.; Shi, F.; Zhang, X. Reversible pH-Responsive Surface: From Superhydrophobicity to Superhydrophilicity. *Adv. Mater.* **2005,** *17*, 1289–1293.
3. Wang, R.; Hashimoto, K.; Fujishima, A.; Chikuni, M.; Kojima, E.; Kitamura, A.; Shimohigoshi, M.; Watanabe, T. Light-Induced Amphiphilic Surfaces. *Nature* **1997,** *388*, 431–432.
4. Takei, Y. G.; Aoki, T.; Sanui, K.; Ogata, N.; Sakurai, Y.; Okano, T. Dynamic Contact-Angle Measurement of Temperature-Responsive Surface-Properties for Poly(*N*-isopropylacrylamide) Grafted Surfaces. *Macromolecules* **1994,** *27*, 6163–6166.
5. Zhao, B.; Brittain, W. J. Synthesis, Characterization, and Properties of Tethered Polystyrene-*b*-Polyacrylate Brushes on Flat Silicate Substrates. *Macromolecules* **2000,** *33*, 8813–8820.
6. Jiang, Y. G.; Wang, Z. Q.; Yu, X.; Shi, F.; Xu, H. P.; Zhang, X.; Smet, M.; Dehaen, W. Self-Assembled Monolayers of Dendron Thiols for Electrodeposition of Gold Nanostructures: Toward Fabrication of Superhydrophobic/Superhydrophilic Surfaces and pH-Responsive Surfaces. *Langmuir* **2005,** *21*, 1986–1990.
7. Chen, M.; Dong, M.; Havelund, R.; Regina, V. R.; Meyer, R. L.; Besenbacher, F.; Kingshott, P. Thermo-Responsive Core-Sheath Electrospun Nanofibers From Poly(*N*-isopropylacrylamide)/Polycaprolactone Blends. *Chem. Mater.* **2010,** *22*, 4214–4221.
8. Wang, X. M.; Zeevi, S.; Kharitonov, A. B.; Katz, E.; Willner, I. Probing Photoinduced Electron Transfer Reactions by *In Situ* Electrochemical Contact Angle Measurements. *Phys. Chem. Chem. Phys.* **2003,** *5*, 4236–4241.
9. Sun, T. L.; Feng, L.; Gao, X. F.; Jiang, L. Bioinspired Surfaces with Special Wettability. *Acc. Chem. Res.* **2005,** *38*, 644–652.
10. Callies, M.; Quere, D. On Water Repellency. *Soft Matter* **2005,** *1*, 55–61.
11. Ercole, F.; Davis, T. P.; Evans, R. A. Photo-Responsive Systems and Biomaterials: Photochromic Polymers, Light-Triggered Self-Assembly, Surface Modification, Fluorescence Modulation and Beyond. *Polym. Chem.* **2010,** *1*, 37–54.
12. Sudesh Kumar, G.; Neckers, D. C. Photochemistry of Azobenzene-Containing Polymers. *Chem. Rev.* **1989,** *89*, 1915–1925.
13. Gorostiza, P.; Isacoff, E. Y. Optical Switches for Remote and Noninvasive Control of Cell Signaling. *Science* **2008,** *322*, 395–399.
14. Hugel, T.; Holland, N. B.; Cattani, A.; Moroder, L.; Seitz, M.; Gaub, H. E. Single-Molecule Optomechanical Cycle. *Science* **2002,** *296*, 1103–1106.

15. Kobatake, S.; Takami, S.; Muto, H.; Ishikawa, T.; Irie, M. Rapid and Reversible Shape Changes of Molecular Crystals on Photoirradiation. *Nature* **2007,** *446*, 778–781.
16. Yoshino, T.; Kondo, M.; Mamiya, J.; Kinoshita, M.; Yu, Y. L.; Ikeda, T. Three-Dimensional Photomobility of Crosslinked Azobenzene Liquid-Crystalline Polymer Fibers. *Adv. Mater.* **2010,** *22*, 1361–1363.
17. Yu, Y. L.; Nakano, M.; Ikeda, T. Directed Bending of a Polymer Film by Light—Miniaturizing a Simple Photomechanical System Could Expand Its Range of Applications. *Nature* **2003,** *425*, 145–145.
18. Hosono, N.; Kajitani, T.; Fukushima, T.; Ito, K.; Sasaki, S.; Takata, M.; Aida, T. Large-Area Three-Dimensional Molecular Ordering of a Polymer Brush by One-Step Processing. *Science* **2010,** *330*, 808–811.
19. Klajn, R.; Wesson, P. J.; Bishop, K. J. M.; Grzybowski, B. A. Writing Self-Erasing Images using Metastable Nanoparticle "Inks". *Angew. Chem., Int. Ed.* **2009,** *48*, 7035–7039.
20. Raimondo, C.; Reinders, F.; Soydaner, U.; Mayor, M.; Samori, P. Light-Responsive Reversible Solvation and Precipitation of Gold Nanoparticles. *Chem. Commun.* **2010,** *46*, 1147–1149.
21. Klajn, R.; Bishop, K. J. M.; Grzybowski, B. A. Light-Controlled Self-Assembly of Reversible and Irreversible Nanoparticle Suprastructures. *Proc. Natl. Acad. Sci. U.S.A.* **2007,** *104*, 10305–10309.
22. del Barrio, J.; Oriol, L.; Sanchez, C.; Serrano, J. L.; Di Cicco, A.; Keller, P.; Li, M. H. Self-Assembly of Linear-Dendritic Diblock Copolymers: From Nanofibers to Polymersomes. *J. Am. Chem. Soc.* **2010,** *132*, 3762–3769.
23. Jiang, D. L.; Aida, T. Photoisomerization in Dendrimers by Harvesting of Low-Energy Photons. *Nature* **1997,** *388*, 454–456.
24. Li, L. S.; Jiang, H. Z.; Messmore, B. W.; Bull, S. R.; Stupp, S. I. A Torsional Strain Mechanism To Tune Pitch in Supramolecular Helices. *Angew. Chem., Int. Ed.* **2007,** *46*, 5873–5876.
25. Ichimura, K.; Oh, S. K.; Nakagawa, M. Light-Driven Motion of Liquids on a Photoresponsive Surface. *Science* **2000,** *288*, 1624–1626.
26. Feng, C. L.; Zhang, Y. J.; Jin, J.; Song, Y. L.; Xie, L. Y.; Qu, G. R.; Jiang, L.; Zhu, D. B. Reversible Wettability of Photoresponsive Fluorine-Containing Azobenzene Polymer in Langmuir−Blodgett Films. *Langmuir* **2001,** *17*, 4593–4597.
27. Jiang, W. H.; Wang, G. J.; He, Y. N.; Wang, X. G.; An, Y. L.; Song, Y. L.; Jiang, L. Photo-Switched Wettability on an Electrostatic Self-Assembly Azobenzene Monolayer. *Chem. Commun.* **2005,** 3550–3552.
28. Lim, H. S.; Han, J. T.; Kwak, D.; Jen, M.; Cho, K. Photoreversibly Switchable Superhydrophobic Surface with Erasable and Rewritable Pattern. *J. Am. Chem. Soc.* **2006,** *128*, 14458–14459.
29. He, J. H. Electrospinning: The Big World of Small Fibers. *Polym. Int.* **2007,** *56*, 1321–1322.
30. Lu, X. F.; Wang, C.; Wei, Y. One-Dimensional Composite Nanomaterials: Synthesis by Electrospinning and Their Applications. *Small* **2009,** *5*, 2349–2370.
31. Agarwal, S.; Wendorff, J. H.; Greiner, A. Progress in the Field of Electrospinning for Tissue Engineering Applications. *Adv. Mater.* **2009,** *21*, 3343–3351.
32. Papenburg, B. J.; Vogelaar, L.; Bolhuis-Versteeg, L. A. M.; Lammertink, R. G. H.; Stamatialis, D.; Wessling, M. One-Step Fabrication of Porous Micropatterned Scaffolds To Control Cell Behavior. *Biomaterials* **2007,** *28*, 1998–2009.
33. Uto, K.; Yamamoto, K.; Hirase, S.; Aoyagi, T. Temperature-Responsive Cross-Linked Poly(ε-caprolactone) Membrane That Functions near Body Temperature. *J. Controlled Release* **2006,** *110*, 408–413.
34. Dorman, G.; Prestwich, G. D. Benzophenone Photophores in Biochemistry. *Biochemistry* **1994,** *33*, 5661–5673.
35. Whitesides, G. M.; Laibinis, P. E. Wet Chemical Approaches to the Characterization of Organic-Surfaces—Self-Assembled Monolayers, Wetting, and the Physical Organic-Chemistry of the Solid Liquid Interface. *Langmuir* **1990,** *6*, 87–96.
36. Bain, C. D.; Whitesides, G. M. Modeling Organic-Surfaces with Self-Assembled Monolayers. *Angew. Chem., Int. Ed. Engl.* **1989,** *28*, 506–512.
37. Siewierski, L. M.; Brittain, W. J.; Petrash, S.; Foster, M. D. Photoresponsive Monolayers Containing In-Chain Azobenzene. *Langmuir* **1996,** *12*, 5838–5844.
38. Moller, G.; Harke, M.; Motschmann, H.; Prescher, D. Controlling Microdroplet Formation by Light. *Langmuir* **1998,** *14*, 4955–4957.
39. Akiyama, H.; Tamada, K.; Nagasawa, J.; Abe, K.; Tamaki, T. Photoreactivity in Self-Assembled Monolayers Formed from Asymmetric Disulfides Having Para-Substituted Azobenzenes. *J. Phys. Chem. B* **2003,** *107*, 130–135.
40. Quéré, D. Wetting and Roughness. *Annu. Rev. Mater. Res.* **2008,** *38*, 71–99.
41. Xin, B.; Hao, J. Reversibly Switchable Wettability. *Chem. Soc. Rev.* **2010,** *39*, 769–782.
42. Rosario, R.; Gust, D.; Garcia, A. A.; Hayes, M.; Taraci, J. L.; Clement, T.; Dailey, J. W.; Picraux, S. T. Lotus Effect Amplifies Light-Induced Contact Angle Switching. *J. Phys. Chem. B* **2004,** *108*, 12640–12642.
43. Fu, Q.; Rama Rao, G. V.; Basame, S. B.; Keller, D. J.; Artyushkova, K.; Fulghum, J. E.; López, G. P. Reversible Control of Free Energy and Topography of Nanostructured Surfaces. *J. Am. Chem. Soc.* **2004,** *126*, 8904–8905.
44. Jeong, H. E.; Kwak, M. K.; Park, C. I.; Suh, K. Y. Wettability of Nanoengineered Dual-Roughness Surfaces Fabricated by UV-Assisted Capillary Force Lithography. *J. Colloid Interface Sci.* **2009,** *339*, 202–207.
45. Wang, N.; Zhao, Y.; Jiang, L. Low-Cost, Thermoresponsive Wettability of Surfaces: Poly(*N*-isopropylacrylamide)/Polystyrene Composite Films Prepared by Electrospinning. *Macromol. Rapid Commun.* **2008,** *29*, 485–489.
46. Lim, H. S.; Kwak, D.; Lee, D. Y.; Lee, S. G.; Cho, K. UV-Driven Reversible Switching of a Roselike Vanadium Oxide Film between Superhydrophobicity and Superhydrophilicity. *J. Am. Chem. Soc.* **2007,** *129*, 4128–4129.